Prediction of Liquation Crack Initiation at HAZ of Laser Weldment Based on Strain Analysis at Elevated Temperature

by Motomichi Yamamoto[1*], Kenji Shinozaki[2], Mitsuru Kitamura[1], Makoto Shirai[3]

[1]Department of Social and Environmental Engineering, Graduate School of Engineering, Hiroshima University, 1-4-1 Kagamiyama, Higashi-Hiroshima, Hiroshima 739-8527, Japan
E-MAIL: myama@naoe.hiroshima-u.ac.jp
[2]Department of Mechanical System Engineering, Graduate School of Engineering, Hiroshima University, 1-4-1 Kagamiyama, Higashi-Hiroshima, Hiroshima 739-8527, Japan
E-MAIL: kshino@hiroshima-u.ac.jp
[3]National Space Development Agency of Japan
World Trade Center Bldg, 2-4-1, Hamamatsu-cho, Minato-ku, Tokyo 105-8060, Japan

ABSTRACT

The purpose of this study is to develope the prediction method of liquation crack initiation in HAZ of laser weldment. Thermal two dimensional strain analyses were performed by FEM for bead-on-plate welding in order to obtain the plastic strain at elevated temperature in HAZ of the laser weldment. From these results, it became clear that the plastic strain at elevated temperature affected liquation crack initiation in HAZ, and it could be proposed that the critical strain, which controlled liquation crack initiation, existed. Moreover, an attempt was made to develop thermal and dynamic three dimensional strain analysis method for the laser weldment in order to obtain the plastic strain at elevated temperature in HAZ of the laser weldment in more detail and precisely.

KEYWORDS

liquation crack, laser welding, three dimensional strain analysis, plastic strain at elevated temperature

1. Introduction

In recent years, since laser beam welding has many excellent abilities such as low deformation, deep penetration, high speed in air and so on, it attracts attentions of many kinds of industries instead of a conventional welding method. However, some researchers indicated that liquation cracking easily occurred in HAZ of laser weldments. From these studies, it became clear that the bead shape affected liquation crack initiation in HAZ strongly, and liquation cracks in HAZ initiated mainly at neck zone of penetration of weld bead [1~4].

In this study, thermal two dimensional elastoplastic strain analyses by FEM were carried out to study the distribution of the strain in HAZ at elevated temperature in order to develope the prediction method of liquation crack initiation in HAZ of laser weldment. Furthermore, a new type of thermal three dimensional elastoplastic strain analysis method by FEM was investigated and proposed in order to obtain the strain at elevated temperature in HAZ of laser weldments in more detail and accurately.

2. Elastoplastic strain analyses at elevated temperature

2.1 Modeling for two dimensional analysis

Thermal two dimensional strain analyses were carried out on bead-on-plate laser welding by using symmetrical 1/2 model as shown in Fig.1. Inconel 718 with a thickness of 5mm was used for the bead-on-plate laser welding.

Five symmetrical models shown in Fig.2 were employed for investigating the effect of the curvature of the neck zone of the weld bead on the cross section. Figure 3 shows the FEM model of Model-A and boundary conditions for the strain analysis. The temperatures of weld beads shown as hatched parts in Fig.2 increased from the room temperature up to the melting point (1617K) for a short time corresponding to the welding speed as shown in Fig.4. The weld bead was meshed in a small size especially near the fusion boundary. The A-area of the 200μm distance from the grain boundary, was automatically meshed in a size of about 10μm, the B-area was meshed in a size of about 50μm.

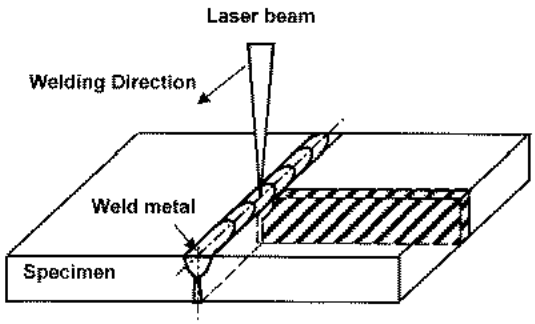

Fig.1 Shematic illustration of bead-on-plate laser welding

2.2 Modeling for three dimensional analysis

In this analysis, two types of FEM models were employed for U-type hot cracking test. One is the large scale

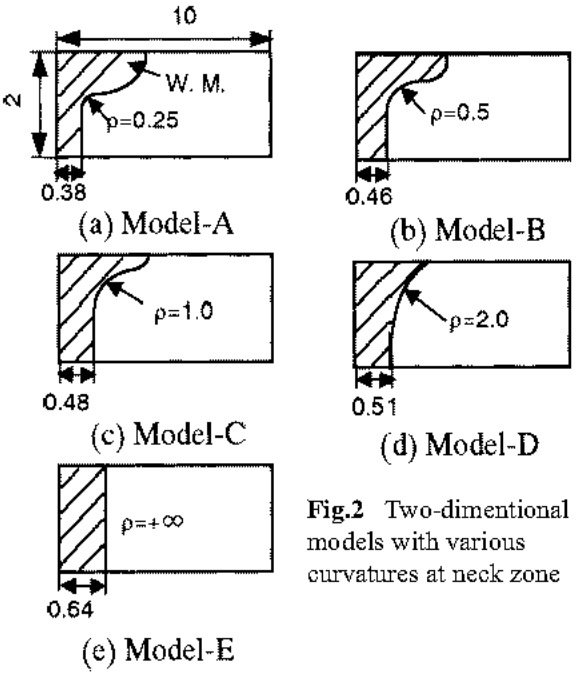

Fig.2 Two-dimentional models with various curvatures at neck zone

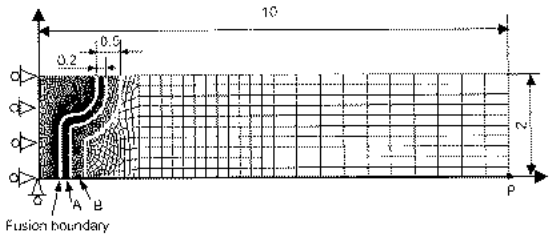

Fig.3 FEM model of Model-A and boundary condition

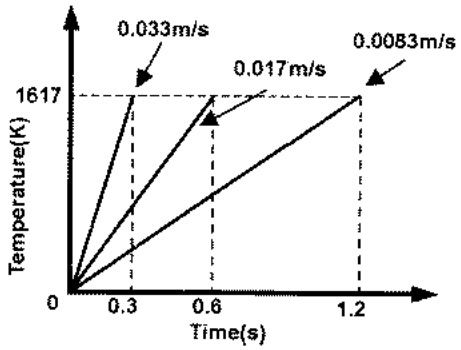

Fig.4 Heat input method

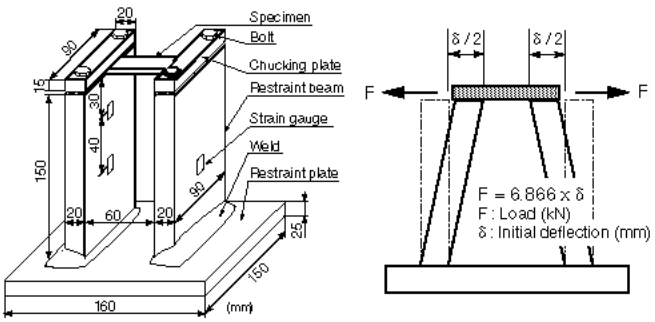

Fig.5 Configuration of U-type hot cracking test device

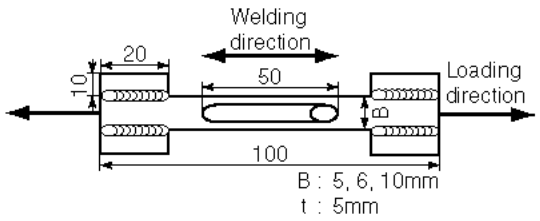

Fig.6 Shape and size of specimen

model for adapting actual large structures, and the other is the small scale model for evaluating the strain at very small local regions in the future.

The configuration of U-type hot cracking test device is shown in Fig.5. The testing sequence is explained as follows. First, two restraint beams are bent within the elastic limit by the external load, and then the specimen is fixed between two restraint beams by chucking plates. When the external load is released, the internal pre-tensile load (F) is applied on the specimen dependent on the initial deflection (δ) as shown in Fig.5. The shape and size of the specimen is shown in Fig.6. The welding direction was parallel to the loading direction, and the bead length was 50mm. Inconel 718 with a thickness of 5mm was used for U-type hot cracking test.

Three dimensional symmetrical 1/2 models for strain analyses are shown in Fig.7. The meshing of large scale and small scale models of the specimen between two restraint beams are shown in Fig.7(a) and (b). Heat transfer analyses were performed by moving the heat source from 'Start' point to 'End' point shown in Fig.7. Element sizes in the weld bead and HAZ for heat transfer analyses were 0.25mm in the welding (X) direction, 0.2mm in the width (Y) direction, 0.2mm in the thickness (Z) direction on the large scale model, and 0.1mm x 0.1mm x 0.2mm on the small scale model. Element sizes for strain analyses were bigger than these of the heat transfer analysis models in the welding (X) direction both of the large scale model and small scale model in order to reduce calculation time.

Young's modulus of the both ends

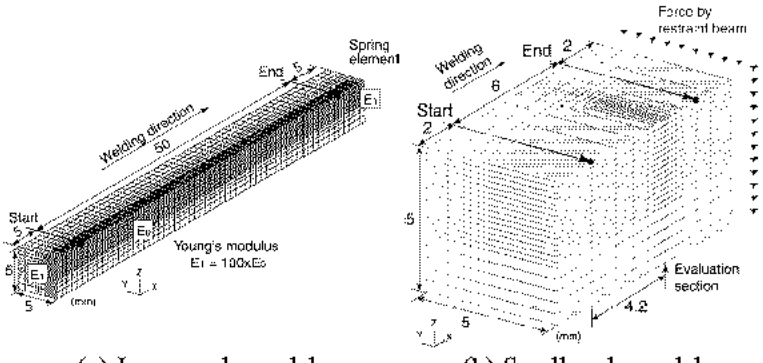

(a) Large scale model **(b)** Small scale model

Fig.7 Models for strain analysis

of the large scale model was 100 times larger than that of the ordinary part, and spring elements with the same stiffness as two restraint beam were attached to the end of the model as shown in Fig.7(a). On the other hand, the analysis with the small scale model was performed by giving the force obtained from tested results to the end of the model as shown in Fig.7(b).

The shape of the heat source and the location of the heat source on the cross section for the small scale model are shown schematically in Fig.8. On the surface part, the heat source with the rectangular solid shape was given in consideration of molten metal convection. And on the middle part, the cylindrical heat source was given in consideration of occurrence of the key hole during welding, and on the bottom of the key hole, the solid heat source was given as well as the surface part. Because of the occurrence of the dimple at the top of key hole on the surface of the specimen, the heat source was not given at the part. In consideration of occurrence of the key hole and the dimple, evaporation of molten metal and so on, the temperature-dependent heat transfer coefficients were given on each surface of the analysis model as shown in Fig.9.

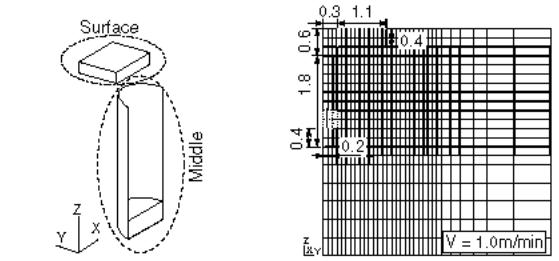

(a) Shape of heat surce **(b)** Location of heat surce on cross section

Fig.8 Shape and location of heat surce of small scale model

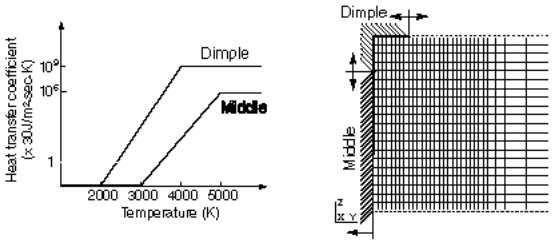

(a) Temperature-dependent heat transfer coefficient **(b)** Setting surfaces on cross section

Fig.9 Method of setting heat transfer coefficient

2.3 Temperature-dependent properties of Inconel 718

Properties of Inconel 718 used for analyses are shown in Table 1. Under the melting point (1617K), specific heat and thermal conductivity are temperature-dependent, and over the melting point (1617K), these are constant. The data over 1450K are assumed. Heat transfer coefficient is the data between Inconel 718 and air, and latent heat is the data assumed from chemical composition of Inconel 718 used for test.

In the strain analysis, the molten metal was treated as the very soft elastic body. Therefore the Young's modulus and yield stress were decreased until the melting point (1617K), after that Young's modulus was kept as very small constant value, and yield stress was increased rapidly over the melting point.

Table 1 Prooerties of Inconel 718 used for analyses

Temperature (K)	294	366	477	589	700	811	922	1033	1144
Specific heat (J/kg· K)	430	-	475	-	530	-	590	-	645
Thermal conductivity (W/m· K)	11.4	-	14.4	-	17.9	-	21.4	-	24.9
Young's modulus (GPa)	200	196	190	184	178	171	163	154	139
poisson ratio	0.30	0.29	0.28	0.278	0.277	0.28	0.283	0.309	0.336
Thermal expansion coefficient (x10⁻⁶/K)	12.20	13.03	13.80	14.00	14.36	14.90	15.43	-	17.45
Yield stress (MPa)	1125	1105	1085	1065	1045	1020	965	800	656
Density (kg/m³)	8220								
Heat transfer coefficient (J/m² sec· K)	30								

Temperature (K)	1255	1366	1450	1534	1607	1617	1800	2000
Specific heat (J/kg· K)	-	700	723	746	-	769	769	769
Thermal conductivity (W/m· K)	-	28.7	30.1	31.6	-	33	33	33
Young's modulus (GPa)	120	99	78	57	-	20	20	20
poisson ratio	0.368	0.4	0.4	0.4	-	0.4	0.4	0.4
Thermal expansion coefficient (x10⁻⁶/K)	-	18.43	18.6	19.0	19.4	0	0	0
Yield stress (MPa)	474	263	112.5	112.5	-	112.5	1038	2051
Density (kg/m³)	8220							
Heat transfer coefficient (J/m² sec· K)	30							

3. Results and discussions

3.1 Experimental verification of three dimensional analysis

Examples of the contour of temperature during welding of the large scale model and the small scale model are shown in Fig.10. Molten pool shapes on the surface of models are good agreement with shapes observed in the test. Examples of the contour of maximum temperature on the cross section of the small scale model are shown in Fig.11. White lines in the figures indicate bead shapes obtained by observation, and the boundary between the green and light blue regions is bead shapes by analysis. It is clear from these figures that the bead shape obtained by analysis fits in the shape obtained by observation. By using this proposal

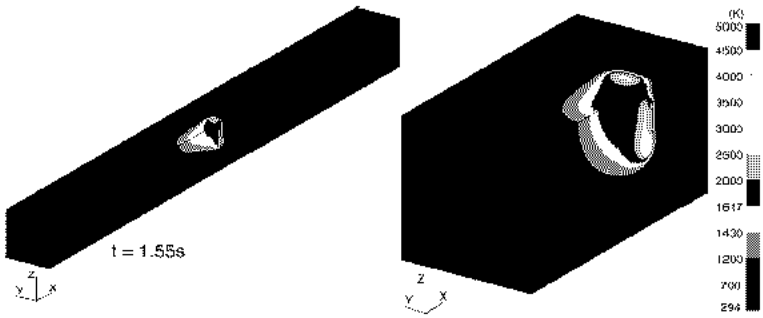

(a) Large scale model **(b)** Small scale model

Fig.10 Contour of temperature during welding

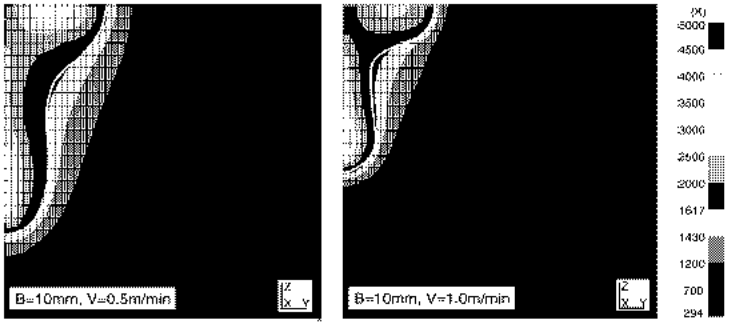

(a) B−10mm, V−0.5m/min (b) B−10mm, V−1.0m/min

Fig.11 Contour of temperature of small scale model

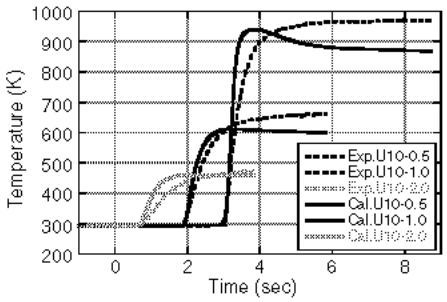

Fig.12 Temperature changes during welding

analysis method, even if the welding speed and specimen width are changed, the bead shape is able to be reproduced well with the constant thermal efficiency and the constant rate of the heat input based on experimental results.

The temperatures during welding on the bottom surface at the longitudinal center of the specimen are shown in Fig.12. Dotted lines and solid lines indicate tested results and calculated results respectively. It can be seen from the figure that the temperature changes obtained by analyses are good agreement with tested results, although there is a little difference between tested results and calculated results on the inclination of temperature increase and so on.

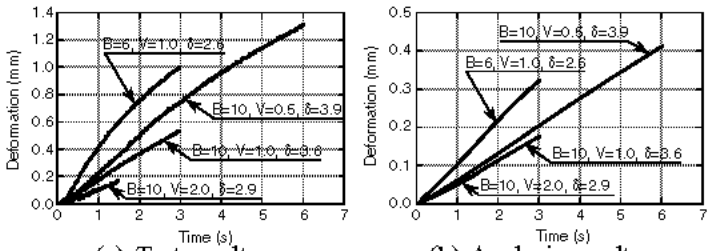

(a) Test results (b) Analysis results

Fig.13 Deformations in welding

Deformations obtained by tests and analyses are shown in Fig.13. It is clear from figures that effects of the specimen width and the welding speed on the deformation of calculated results are good agreement with these of tested results qualitatively. But the deformation obtained by analyses are very small compared quantitatively with that obtained by the test. That is considered as one of the big issue which must be solved immediately in the future.

3.2 Thermal analyses

The width of liquefied temperature range [WLTR : 1434K (grain boundary liquation temperature) ~1617K (melting point)] was used as the factor which have important effect on liquation crack initiation in HAZ. The WLTR obtained by two dimensional analyses from the surface to the bottom in five models with various curvatures are compared in Fig.14. An example of temperature changes during welding on the cross section obtained by three dimensional analysis is shown in Fig.15. The cross section of two dimensional analysis model (full penetration) was divided into three regions, and that of three dimensional analysis model (partial penetration) was divided into four regions as shown in Fig.16.

It is clear from Fig.14 that the WLTR at the Region-II (neck zone) increases as the curvature of the neck zone decreases. It is also evident from Fig.15 that the temperatures in the Region-II (neck

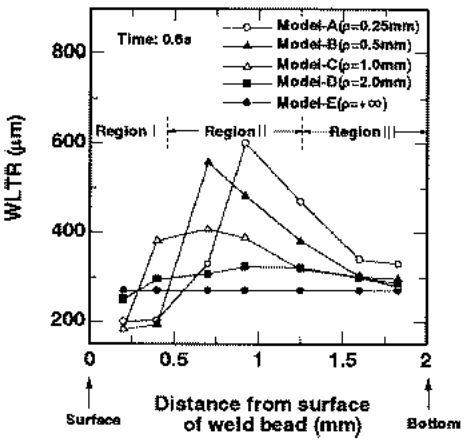

Fig.14 Distribution of WLTR for various curvature of neck zone toward thickness direction

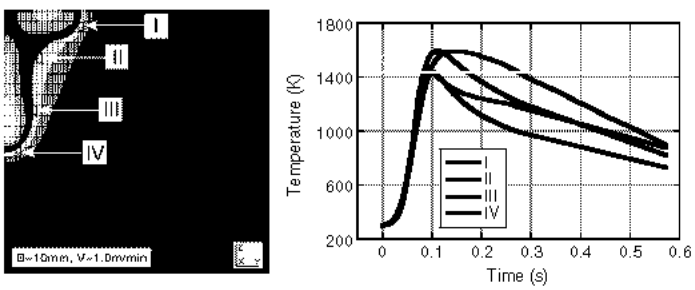

Fig.15 Temperature changes in welding on cross section (small scale model, B−10mm, V−1.0m/min)

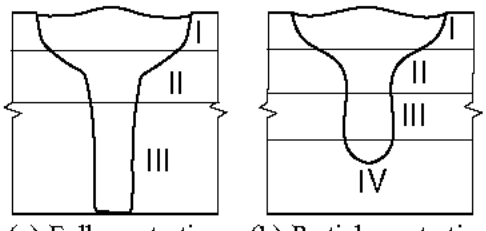

(a) Full penetration (b) Partial penetration

Fig.16 Regions in cross section

zone) and Region-III (just under neck zone) are kept over 1434K for longer time, and cooling speeds from the peak temperature are slower than these in the Region-I and Region-IV. Moreover the WLTR shown light blue in Fig.15 at neck zone is wider than the other regions.

Figure 17 shows the rate of liquation crack initiation on each reagion of cross section of U-type crack initiation test specimens shown in Fig.16(b). It is clear from the figure that the rate of liquation crack initiation is varied on each region, and the rate of the Region-II and Region-III are much larger than these of the Region-I and Region-IV. Results of heat transfer analyses, as mentioned above, can be considered as the one of main reasons for liquation crack initiating easily at neck zone.

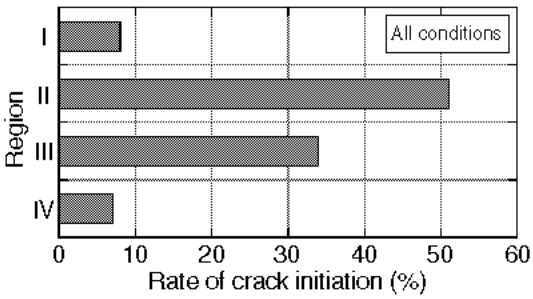

Fig.17 Rate of liquation crack initiation on each region of U-type crack initiation test specimen

3.2 Strain analyses

A plastic strain was used for an evaluating parameter of liquation crack initiation in HAZ, because the crack initiated at elevated temperature (1434K ~ 1617K) and the deformation of weldment was considered as the cause for the crack initiating.

Figure 18 shows distributions of plastic strains of equivalent plastic strain (ε_{pEQ}) and first principle plastic strain (ε_{p1}) of fusion boundary toward thickness direction for Model-A for two dimensional analyses. Figure 19 shows an example of the contour of equivalent plastic strain on the cross section, and Fig.20 shows an example of the distribution of each directional component of plastic strain toward the thickness direction, and locations of evaluated elements on the cross section is shown in Fig.20(b). White dotted lines in Fig.19 indicate bead shapes obtained by analyses. Moreover, Fig.21 shows examples of distributions of maximum and minimum principle plastic strain in HAZ on the cross section. These results shown in Fig.19, Fig.20 and Fig.21 were obtained from three dimensional analyses with the small scale model.

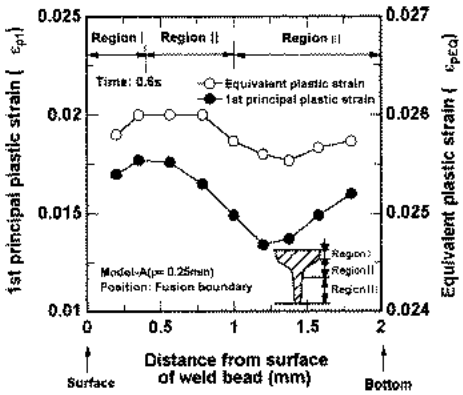

Fig.18 Distribution of plastic strains on fusion boundary toward thickness direction

It can be seen from Fig.18, Fig.19 and Fig.20 that both values of ε_{pEQ} and ε_{p1} at neck zone (Region-II) are bigger than these of other regions. It can be considered as the one of main reasons for liquation crack initiating easily at neck zone as shown in Fig.17. Futhermore, it become clear from the results obtained by three dimensional analyses that the shear strain in the Y-Z direction (γ_{YZ}) also become larger at neck zone and just under neck zone as shown in Fig.20, and components in the welding (X) direction of the maximum and minimum principle plastic strains are very small at neck zone as shown in Fig.21.

The relationship between the average value of plastic strains of $\bar{\varepsilon}_{pEQ}$ and $\bar{\varepsilon}_{p1}$ on fusion boundary and heat input of laser welding are shown in Fig.22. The solid and open marks represent cracking and no cracking respectively. It can be seen from the figure that both $\bar{\varepsilon}_{pEQ}$ and $\bar{\varepsilon}_{p1}$ decrease as the heat input increases. The critical values of plastic

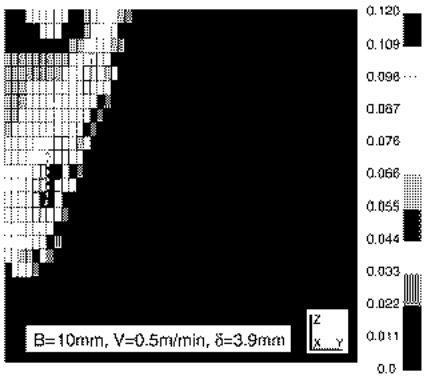

Fig.19 Contour of equivalent plastic strain on cross section

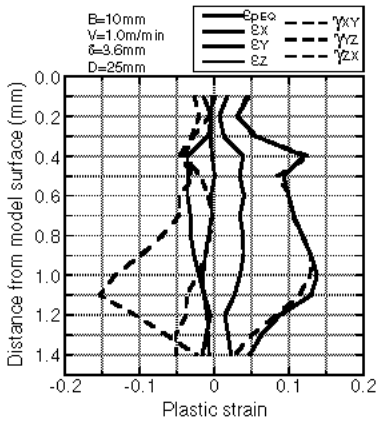

(a) Strain distribution

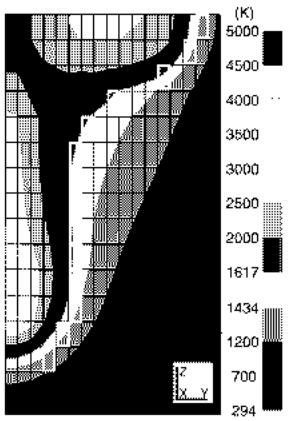

(b) Evaluation elements

Fig.20 Distribution of plastic strain toward thickness direction (B=10mm, v=1.0m/min, δ=3.6mm)

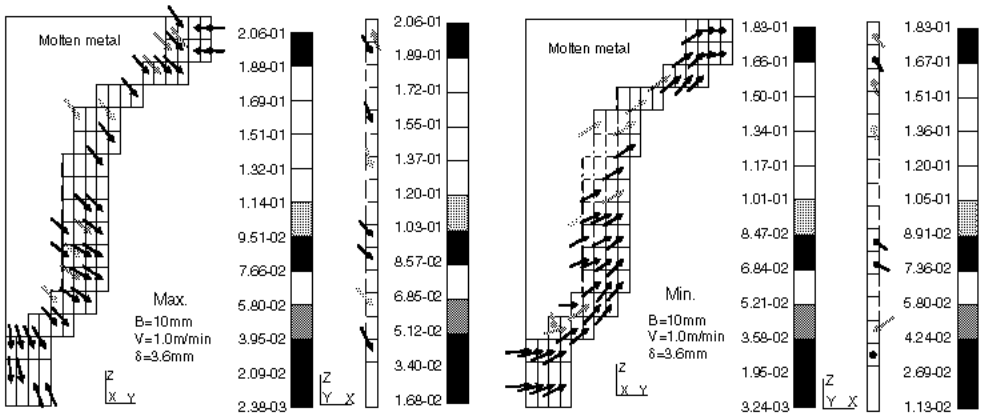

(a) Maximum principle plastic strain (ε_{p1}) **(b)** Minimum principle plastic strain

Fig.21 Distributions of maximum and minimum principle plastic strain in HAZ

strain for $\bar{\varepsilon}_{pEQ}$ and $\bar{\varepsilon}_{p1}$ exist from the result of the occurrence of liquation cracks. Liquation cracks occur when $\bar{\varepsilon}_{pEQ}$ is beyond the critical value of 0.0266 or $\bar{\varepsilon}_{p1}$ is beyond the critical value of 0.0196 in two dimensional analyses. Therefore, it suggests that liquation cracks can be prevented by decreasing the plastic strain at HAZ via increasing the curvature of the neck zone by means of selecting the suitable heat input of laser welding.

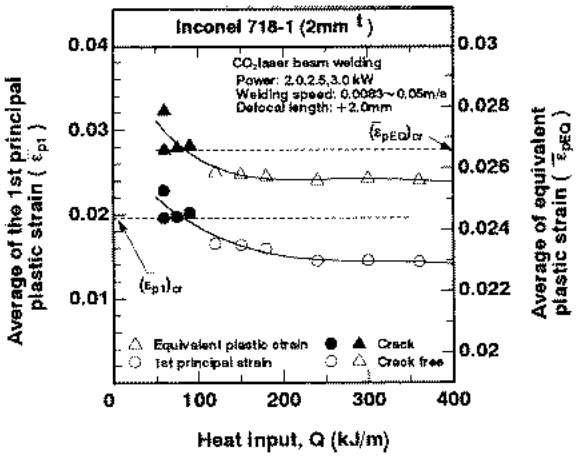

Fig.22 Evaluation for liquation crack initiation in HAZ by using values of plastic strains

4. Conclusion

In this study, an attempt was made to develope the prediction method for liquation crack initiating in HAZ of laser weldment based on the plastic strain at elevated temperature in the crack initiation region obtained by thermal two dimensional elastoplastic strain analyses by FEM. Furthermore, a new type of thermal three dimensional elastoplastic strain analysis method by FEM was investigated and proposed in order to obtain the strain at elevated temperature in HAZ of laser weldments in more detail and accurately. As a result of this study, following conclusions were obtained.

(1) The width of liquefied temperature range (WLTR) at neck zone was larger than at other regions and was held in higher temperature for more time than at other regions. The WLTR at neck zone increased as the curvature of neck zone decreased.

(2) Both the equivalent plastic strain ($\bar{\varepsilon}_{pEQ}$) and the first principal plastic strain ($\bar{\varepsilon}_{p1}$) at neck zone increased with decrease of the curvature at the neck zone. From this result, it was considered that liquation cracks initiated easily at neck zone in HAZ.

(3) It became clear that the critical plastic strains ($\bar{\varepsilon}_{pEQ}, \bar{\varepsilon}_{p1}$) exists. And the prediction method for liquation crack initiating in HAZ of laser weldment based on the plastic strain at elevated temperature in the crack initiation region could be proposed.

(4) From results of three dimensional analyses, by using this proposal analysis method, the bead shape can be reproduced very well with the constant analysis condition, and the strain at HAZ of laser weldments can be calculated in detail.

References

[1] K. Shinozaki, X. Luo, H. Ariyoshi, H. Kuroki and M. Shirai: Quarterly Journal of the Japan Welding Society, Vol.17, No.2 (1999), pp.279-285.

[2] K. Shinozaki, X. Luo, H. Ariyoshi, H. Kuroki and M. Shirai: Quarterly Journal of the Japan Welding Society, Vol.17, No.2 (1999), pp.286-293.

[3] K. Nishimoto, I. Woo, T. Ogita and M. Shirai: Quarterly Journal of the Japan Welding Society, Vol.19, No.2 (2001), pp.308-316.

[4] K. Nishimoto, I. Woo and M. Shirai: Quarterly Journal of the Japan Welding Society, Vol.19, No.3 (2001), pp.480-488.